Study of scattering patterns and subwavelength scale imaging based on finite-sized metamaterials

Schenk, John O.; Fiddy, Michael A.; Zhang, Yuan; Chuang, Yi-Chen

2011

Zhang, Y., Chuang, Y. C., Schenk, J. O., & Fiddy, M. A. (2011). Study of scattering patterns and subwavelength scale imaging based on finite-sized metamaterials. Applied Physics A: Materials Science & Processing, 107(1), 61-69.

https://hdl.handle.net/10356/94379

https://doi.org/10.1007/s00339-011-6738-9

Study of scattering patterns and sub-wavelength scale imaging based on finite-sized metamaterials

Yuan Zhang

Electromagnetics Academy at Zhejiang University, Zhejiang University, Hangzhou 310027, China

Yi-Chen Chuang

School of Electrical and Electronic Engineering, Nanyang Technological University, 50 Nanyang Avenue, 639798, Singapore

ycchuang@ntu.edu.sg

John O. Schenk and Michael A. Fiddy

Center for Optoelectronics and Optical Communications, University of North Carolina at Charlotte, 9201 University City Blvd, Charlotte, North Carolina 28223, USA

joschenk@uncc.edu; mafiddy@uncc.edu

Abstract

A metamaterial slab, used as a superlens in a sub-wavelength imaging system, is frequently assumed homogeneous. It is the bulk properties of the metamaterial which are responsible for the resolution of the transferred information in the image domain, as a result of high transverse wave-vector coupling. However, how in a discretized metamaterial, individual meta-atoms (i.e. the meta-elements composing a negative index metamaterial slab) contribute to the imaging process is still actively studied. The main aim of this paper is to investigate the consequences of using only a few meta-atoms as a negative index slab-equivalent for sub-wavelength scale imaging. We make a specific choice for a meta-atom and investigate its resonant scattering patterns. We report on how knowledge of these 3D scattering patterns provides a means to understand the transfer of high spatial frequencies and assist with the design an improved negative index slab.

1 Introduction

There has been much interest for the past ten years in the opportunities that metamaterials offer for sub-wavelength scale imaging. When using a metamaterial as an imaging slab having an index close to the ideal n = -1 (i.e. a *superlens*), transverse spatial frequencies, associated with evanescent waves in the propagation direction, get transferred to the image domain through a resonant coupling mechanism [1]. A schematic for this kind of imaging indicating negative refraction is shown in figure 1 with a possible metamaterial design. One normally assumes that the dimensions of individual meta-atoms are much smaller than the operating wavelength (λ) and that an effective

medium approximation [2] can be invoked to allow field averaging. One also assumes that the medium interfaces are very smooth on the scale of the spatial period to be transferred to the image domain. In such cases, the resulting image can be assumed to have been transferred through a homogeneous slab. In practice, constructing meta-atoms that are considerably smaller than the operating wavelength is difficult, especially in the optical spectrum. Consequently, if the dimensions of meta-atoms are not sufficiently smaller than the operating wavelength, an effective medium approximation no longer holds. In this case, one might expect not only a limit to the image resolution but also the need for some processing of the scattered fields measured in the image domain, to recover an image. Scattering *per se* will limit the transfer of high spatial frequencies into the image domain, but the question is how and to what extent? A fundamental question therefore arises as to how scattering from each meta-atom as well as collective scattering modes contribute not only to the bulk properties of the metamaterial, but more importantly, to the quality and resolution of the image that can be computationally reconstructed from image domain measurements.

Of interest in this paper is to deepen our understanding of the limits on high spatial frequency information that can be transferred through propagation and scattering mechanisms in a metamaterial lens when it is made from finite-sized and finite numbers of meta-atoms. To do this, we study the scattered field patterns from a single meta-atom and from small arrays of meta-atoms as a function of incident spatial and temporal frequency.

2 Meta-atoms and their properties

There has been much written on possible choices for individual meta-atom structures and how to control their resonant behavior in order to realize a negative index [3, 4]. The main difficulty is to tune the permittivity (ε) and permeability (μ) resonances in a systematic way and ensure the real parts of ε and μ are negative over a common chosen bandwidth or that both real and imaginary parts satisfy the condition that $\varepsilon''\mu' + \varepsilon'\mu'' < 0$, where $\varepsilon = \varepsilon' + i\varepsilon''$ and $\mu = \mu' + i\mu''$ [5]. Besides, it is essential to prevent any possible loss because even small losses will drastically limit the spatial frequency transfer function [2], rapidly resulting in an image field with no better resolution that a typical lens would provide. The resolution degrades exponentially as a function of $2\pi d/|\log \delta|$ where d is the thickness of the slab and δ is the imaginary part of either the metamaterial lens' permittivity or permeability. In addition, as inhomogeneities of a metamaterial could equate to a loss mechanism, the control of fabrication tolerances is also important, especially for scales that higher transverse wave vectors can couple into. We have focused on one meta-atom structure for the purpose of this paper and describe how its inherent scattering properties contribute to the transfer of propagating and evanescent waves, both as an individual scattering element and as a component in a negative index slab for imaging purposes.

The particular meta-atom we make use of here is a double-layered "*S*"-like structure (figure 2), where the *S* elements are made of copper and printed on the opposite sides of a substrate (FR4, ε= 2.33). The dimensions of this meta-atom are described in figure 2, and the dielectric constant of the materials used is assumed constant as a function of frequency for simplicity. This structure has evolved from earlier work of Kong *et al* [6] and has been modified to allow more flexible control of the ε and μ spectral responses [7]. A connected array of such *S* elements is also referred to as a metallic meandering line [8]. We applied basic circuit theory based on the incident *E* and *H* fields and obtained the corresponding LCR circuit of the *S* structure (figure 3). The S model can be represented as a combination of resistance, capacitance and inductance in a series-parallel circuit, similar to that proposed in [6]. By combining the impedance representation from each contribution arising from the geometry and material properties of the paired *S* structure, an analytic expression for the impedance transfer function of a single meta-atom can be obtained [6,7]. Knowledge of the impedance transfer

function for this single unit cell allows one to identify a number of resonances. Also the effective averaged permittivity and permeability of the *S* structure can be inferred from this complex impedance function, specifically the frequency dependence of the reactance contributions which in turn directly dictate the frequency response of ε and μ. Once ε and μ are known, estimates of the effective complex refractive index (n) of the *S* structure can be deduced from scattering parameters using a variety of approaches (e.g. [9]). We expect the peaks or zeros in the index of refraction and the impedance to be at these resonance frequencies but this does not necessarily occur in practice due to field and mesh averaging [10]. Note that *effective* constitutive parameters, including ε, μ and n, are used in this paper to describe averaged properties of a single or small array of meta-atoms. Defining a refractive index is obviously not a concept one would normally try to assign to a single unit cell, but the "effective negative refractive index" associated with the *S* meta-atom is an averaged quantity just like the impedance and is based on the resonant responses of the equivalent LCR circuits. This unit cell's impedance response is valid for a specific excitation of the *S* structure arising from the incident E_y field whose temporal frequency we assume to be fixed but whose complex amplitude depends on the coherent sum of spatial frequency amplitudes present. We also note that a structure very similar to the proposed here was the subject of a recent publication by Guney *et al* [11], in which they also first considered a single meta-atom's effective constitutive parameters. This single unit cell extraction indicating an effective negative index was based on the homogeneous effective medium approximation described in [10].

In our example, there is a strong impedance resonance at 4.74 GHz but also a total of seven other resonances, some of which are associated with frequencies where this unit cell can be considered as having an effective negative refractive index. The concept of effective negative index can be interpreted as follows. One assumes that positive index materials comprise of atoms that have dipole radiation patterns, and a sheet of dipoles results in a forward propagating wave that experiences approximate a $\pi/2$ phase retardation with respect to the incident wave. This retardation defines a phase velocity slow-down expressed by the parameter we call refractive index. A negative index behavior material has a scattered propagating wave that is phase shifted between $\pi/2$ to π radians which can be considered a phase advance. It is this relative phase advance than manifests itself as a backward wave in a negative index material giving opposing group and phase velocity directions. At 7.83 GHz (see figure 4), we observe a scattered field that is not in phase with the incident wave; the field from a sheet of such meta-atoms would result in a phase advance in the forward direction. This observation indicates the local meta-atom's near field scattering pattern which is responsible for transferring the incident field. Here we assume the incident field has a wide spatial frequency bandwidth corresponding to both propagating and evanescent waves. The modulation of those spatial frequencies depends on the detailed structure of the scattering pattern to different spatial frequencies. Should those reradiated and scattered waves be successfully transferred to the image domain, then knowledge of the bulk transfer function will allow the wave incident initially on the metamaterial to be reconstructed in principle. If the wave originated from a weak rather than strong scatterer, this image wave would be directly proportional to the subwavelength scale features of the scattering object being imaged, i.e. if the first Born approximation holds and if the bulk effective refractive index was also close to $n = -1$.

Effective constitutive parameters are shown for our meta-atom in figure 5. The sign of the black curve in figure 5 indicates where there is a net phase advance and so the effective refractive index of the single meta-atom is negative. Note that ε'' and μ'' are not always positive as they should be for a passive structure [10]. In order to interpret these properties for a unit cell, we studied the structure of the near-field scattered field from a single meta-atom. As seen in figure 4, the very complex scattering pattern that results shows a phase in advance of that of the incident field's amplitude fluctuations. The complexity of the field indicates a field-enhanced multipole response, which one might expect to be capable of transferring different spatial frequencies through the structure. An effective negative index associated with a backward wave can be observed over a range of frequencies. At a temporal frequency associated with an effective negative refractive index, the transfer of amplitude information about spatial frequencies up to some maximum will occur, averaged over the spatial frequency bandwidth. The near field scattering pattern is not likely to be spatial

frequency dependent unless the meta-atom, here a dual *S* structure, has a stronger resonant response at the same temporal frequency but at a different angle of incidence. Thus, for a single unit cell, a projection of the spatial frequency content of the incident wave is transferred, which incorporates some information about evanescent wave amplitudes from sub-wavelength scale features in the scattering object.

3 Arranging clusters of meta-atoms

In this section, we discuss the connection between the properties of a bulk metamaterial and that of a unit cell, based on the scattered field from individual single meta-atom. The scattered field shown in figure 4 from a single meta-atom was obtained using commercial software, COMSOL (v.4.1), which is based on a finite element method. The incident field was a plane polarized wave entering from the right with the *E* field aligned with the *y*-axis. The total field illustrated by the scattered E_y component plus the incident field is shown (figure 4(b)) and compared with the scattered fields, E_x, E_y and E_z (figure 4(c) ~4(e)). We note that within the frequency range corresponding to a negative refractive index, the resonance of the *S* element radiates a scattered field that is itself *asymmetric* in all three dimensions. These field distributions suggest arrangements for modified lattices on which to place each meta-atom, depending on whether strong or weak interaction between units is desirable. In order to ensure a phase advance is sustained and hence an effective negative index behavior predominates, it is important that the scattered fields from individual units maintain their phase advance and that the integrated field from a meta-atom sheet also sustains the phase advance. Positioning adjacent meta-units to maximize coupling with the highest order multipole components of these field patterns will modify the transfer of high spatial frequency information. We have begun to consider combinations of *S*-shaped meta-atoms into larger arrays or clusters and optimize their relative locations, in order to tune the effective negative index and the spatial transmission bandwidth of the bulk material. Based on the amplitudes of the scattered fields in *x*, *y*, and *z* (figure 4(c) ~4(e)), we have found that adjacent meta-atoms need to be much closer in *z* than in *y* and closer in *x* than in *y* in order to ensure uniform coupling and the observation of a backward wave. We have found that there is a minimum size array of meta-atoms, beyond which addition of more meta-atoms no longer significantly alters the properties of that backward wave. The bulk properties for our unit-cell *S* structure are essentially fixed once the number of meta-atoms, N_j in the j^{th} direction have reached $N_x > 2$, $N_y > 20$, $N_z > 30$.

The resonant scattering, as the example shown in figure 4 at 7.83 GHz from a single meta-atom, is associated with a huge field enhancement, in this case having a magnitude of ~30. This can be exploited to compensate for losses in a bulk material. More dilute or sparse arrays will experience less coupling between meta-atoms, which decreases the importance of multipole interactions between meta-atoms but minimizes losses. Unfortunately, such dilute bulk metamaterial will behave as a weak scatterer. This does not mean that it will not transfer subwavelength scaled information into the image domain, but only that, as a weaker scattering structure, there could be a strong background incident wave against which the high resolution information-bearing wave needs to be measured. We have investigated the extent of high spatial frequency transfer one could achieve using just one meta-atom as a single scattering entity playing the role of an effective negative index metamaterial slab. If the meta-units were to be placed periodically, we can expect much more complicated responses which roughly decompose into the responses of a single unit and responses due to the periodicity, as pointed out in [10]. For example, we can expect bandgaps and distorted resonances arising from the periodic component.

4 Single meta-atom superlenses

In figure 6, we illustrate the transfer of information bearing fields through a single meta-atom with an effective negative index in the sense described above. Although this meta-atom has dimensions smaller than the wavelength (see figure 6(a)), a low pass filtered image of a point source can be seen in figure 6(b). The incident wave is coming from the right in these figures. The low-pass filtered image has a resolution comparable to the height of the meta-atom. To transfer higher spatial frequencies, the object field would have to be placed much closer to the meta-atom. We simulated illuminating this meta-atom directly with evanescent waves, i.e. with very high spatial frequency non-propagating fields. We observe that these waves stimulate the resonant behavior at this temporal frequency as expected and generate propagating waves. This is illustrated in figure 7. There is no clear evidence from these numerical experiments that a meta-atom is capable of transferring information that is specific to individual spatial frequencies $k_x > k_0$, for the several choices of increasing k_x that were considered. This is to be expected given the finite sized mesh used in the simulation. Also, physically, the expectation that increasingly high-k evanescent waves decay increasingly rapidly is inevitable and higher multipole responses of the meta-atom also decay rapidly. Even with high local field enhancements due to the resonance, adjacent meta-atoms would still need to be increasingly close to each other in order to couple into them.

In figure 7 we see a resonant response to the evanescent wave's temporal frequency but not its specific spatial frequency. This suggests that it is the actual physical dimensions and properties of each meta-atom (e.g. its effective refractive index), that are the limiting factors to spatial frequency transfer. To further investigate this, simulations were carried out using a perfect $n = -1$ slab having the same dimensions as the substrate of the meta-atom. Figure 8 shows the total fields (i.e. fields containing high spatial frequencies and a component of unscattered incident waves) from the ideal $n = -1$ slab. For these examples, evanescent wave transfer via surface waves is apparent. The surface waves transfer only a limited subset of high spatial frequencies due to the finite size of the slab. Unfortunately, we can only display a limited number of high spatial frequency fields due to software limitations.

Finally, a cluster of 4 by 5 *S* elements was investigated at the resonant frequency for which a phase advance was observed for a single meta-atom (figure 9). This structure, now extended in the direction of the incident field, illustrates the importance of correctly locating each meta-atom to ensure their scattering patterns combine to create a backward wave rather than a forward wave. The array area is large enough to detect a backward wave but one is not evident. We can deduce that the relative spacing of the unit cells has not lead to a net phase advance with respect to the surrounding incident wave. Also, E_x and E_z show asymmetry and the field associated with this structure and the incident field almost perfectly destructively interfere as can be seen in the full field plot (figure 9(a)). One can threshold these field patterns to try to detect some evidence of high spatial frequency transfer through this thin structure. An apparent image of the field exiting a subwavelength scale slit can be observed but only after thresholding (figure 9(e)). The important conclusion from this is that despite the finite size of the bulk metamaterial, the field representing the image is difficult to extract from the total field. Since only fields are ever observed when imaging, then it is easy to be misled about what fields represent the image, when complicated scattered and diffracted field patterns are so prevalent.

5 Discussion

In the extreme limit of vanishingly small meta-atoms on the scale of the wavelength, the physical model of resonant amplification of a wide spatial spectrum of evanescent waves is reasonable. However, fabricating meta-atoms that are a lot smaller than the wavelength will always be a challenge, especially for use at optical frequencies. Each meta-atom, depending on its design, generates a complicated 3D scattering pattern which is only comparable to that of a simple dipole-like radiation pattern for the primary impedance resonance at some distance from its center beyond the

near field. Several resonances are likely for a single meta-atom, especially of the type described here. Our *S* structure exhibited a phase advance at one of these resonant frequencies and has the necessary response to build a negative index metamaterial. This out-of-phase scattered wave was associated with a spatially asymmetric resonance of the meta-atom. The complexity of the scattering patterns makes the location of adjacent meta-atoms critical in order to guarantee the desired properties of a bulk metamaterial and this continues to be quite a challenge.

A large local field enhancement is observed when resonant scattering occurs and this can be exploited to sustain the transfer of information-bearing waves through the structure. We argued that a single meta-atom can have an effective refractive index even though subwavelength in scale, and that all spatial frequencies, including those associated with evanescent waves, do excite each meta-atom as well as generating propagating waves. The problem for high resolution imaging is that it is not clear if the scattered wave encodes different spatial frequencies. The extreme case of imaging from a single meta-atom was compared with the results from a perfect $n = -1$ slab of the same size. Very high spatial frequencies from a sub-wavelength scale feature located very close to the front face of a negative index slab lens, can be transferred to the image domain. Lower spatial frequencies, both evanescent and propagating, cannot be well represented and transferred with fidelity from such a small structure. The physical size of the meta-atom and the field pattern of the highest order contributing multipole will place limits on the ultimate resolution one might achieve. This limitation is well known when meta-atoms are located periodically and usually diffraction effects are invoked to explain this size-related resolution limit (e.g. [10]). For the highest spatial frequencies and a perfect $n = -1$ slab, one expects a transfer of very high transverse wave vectors. Lower spatial frequencies, propagating or not, may not interact strongly with a single meta-atom because of its relatively small scattering cross section. Consequently, a weakly scattering single unit or small cluster of meta-atoms may function as expected for a perfect lens but the presence of the total field makes it difficult to measure the scattered field. The positive consequence of this is that if scattering is well approximated by the first Born approximation, then the interpretation of the measured field as an image of the scattering object's constitutive parameters is straightforward.

6 Conclusions

We have investigated the role of scattering from meta-atoms to try to deepen our understanding of how subwavelength scale information, i.e. high spatial frequencies encoded by evanescent waves, get transferred through a real metamaterial negative index slab. Information-bearing fields are transferred through propagation and resonant scattering by each meta-atom in the metamaterial. However, the anisotropic S structure will only have an effective index of $n = -1$ for one polarization component and generates similar propagating scattered waves for both incident propagating and evanescent waves. The choice of meta-atom dictates the near-field scattering amplitudes and the 3D structure of these fields provides a means to determine the separations between meta-atoms in *x*, *y* and *z* to build a cluster whose properties do not change when more meta-atoms are added. The coupling of multipole fields between meta-atoms is responsible for the subtle differences in how sub-wavelength scale information is transferred to the image domain; the relatively coarse mesh size in simulations makes this difficult to investigate. A metamaterial composed of unit cells of the type used here will effectively transfer the high wave vectors that are coupled into the cluster and experience phase shifts corresponding to an effective negative index. This will apply to all spatial frequency contributions from the entire *volume* of the object for that orientation of the individual *S* element or bulk metamaterial. At other incident angles, reflection and dispersion losses will have reduced their intensity in the image domain. Rotating the object will generate another but different output field in the image domain encoding high spatial frequencies. From a set of these field measurements, one can calculate the high resolution image. The closer the index to $n = -1$ the wider the spatial frequency bandwidth contributing to the object projection information present in the field measured in the image domain.

The field in the image domain may not be proportional to the permittivity or refractive index of the scattering object if the first Born approximation is not valid [12] and an inverse scattering algorithm will be needed. It is thus highly likely that the measured fields will need to be numerically processed to recover a high resolution image and this suggests that one might be able to improve the resolution even more, through further computational steps. The well-known Generalized Sampling Theorem [13, 14], provides a means to compute a high resolution image from a set of independent lower resolution images. The discrete structure of the negative index metamaterial will limit the resolution but as a result of propagation and scattering through the metamaterial, higher spatial frequencies get differently encoded as a function of the angular limitations imposed on near $n = -1$ properties due to the metamaterials anisotropy. Nevertheless, a set of relatively low resolution image fields can provide a set of independent data for applying the generalized sampling theorem and an inverse scattering procedure, from which a high resolution image can be computed.

Acknowledgements

The authors are grateful for support from National Research Foundation of Singapore, grant number NRF-G-CRP 2007- 01. JOS and MAF would also like to acknowledge DE-FG02-06CH11460.

List of references

1. J. B. Pendry, Physical Review Letters **85,** 3966 (2000)
2. D. Smith, Appl. Phys. Lett. **82,** 1506 (2003)
3. C. M. Soukoulis, J. Zhou, T. Koschny, M. Kafesaki, and E. N. Economou, Journal of Physics: Condensed Matter **20,** 304217 (2008)
4. C. M. Soukoulis and M. Wegener, Nature Photonics, doi: 10.1038/nphoton.2011.154 (2011)
5. A. Boardman, N. King, and L. Velasco, Electromagnetics **25,** 365 (2005)
6. H. Chen, L. Ran, J. Huangfu, X. Zhang, K. Chen, T. M. Grzegorczyk, and J. A. Kong, Physical Review E **70,** 057605 (2004)
7. J. O. Schenk, Phd Dissertation, University of North Carolina at Charlotte (2010)
8. L. Fu, H. Schweizer, H. Graebeldinger, H. Guo, N. Liu, and H. Giessen, Metamaterials' 2008, Pamplona, Spain, 362 (2008)
9. J. Yang, Appl. Phys. Lett. **97,** 061102 (2010)
10. T. Koschny, P. Markoš, E. N. Economou, D. R. Smith, D. C. Vier, and C. M. Soukoulis, Physical Review B **71,** 245105 (2005)
11. D. Ö. Güney, T. Koschny, M. Kafesaki, and C. M. Soukoulis, Opt. Lett. **34,** 506 (2009)
12. M. A. Fiddy and M. Testorf, Optics Express **14,** 2037 (2006)
13. A. Papoulis, IEEE Transactions on Circuits and Systems **24,** 652 (1977)
14. M. E. Testorf and M. A. Fiddy, *Chapter 5 - Superresolution Imaging—Revisited*, in *Advances in Imaging and Electron Physics*; W.H. Peter, Editor, p. 165-218, (Elsevier, 2010)

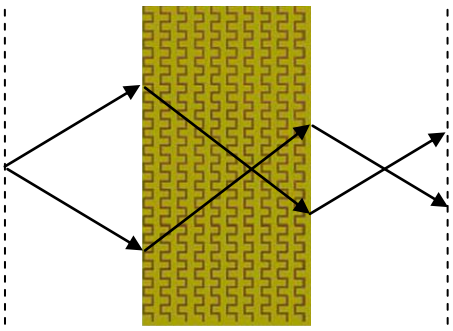

Figure 1. Basic geometry of an imaging system using a metamaterial slab having an index close to the ideal $n = -1$

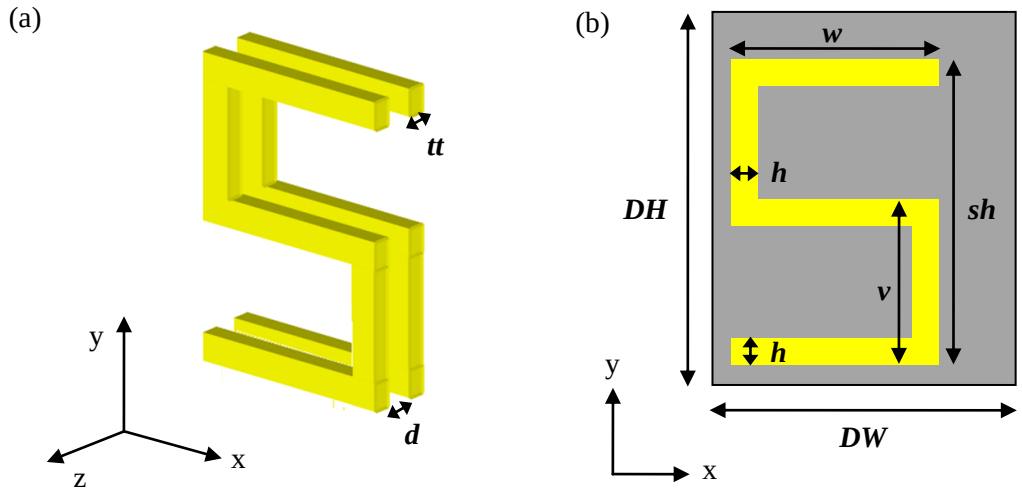

Figure 2. Proposed double-layered "*S*"-like structure (a) with dimensions indicated, where *w*=*v*=7 mm, *sh*=13 mm, *h*=1 mm, *tt*=38 μm, and *d*=0.5 mm. This structure is made of copper and is printed on the opposite sides of a dielectric substrate (FR4, ε=2.33) with *DH*=16 mm and *DW*=13 mm (indicated by the gray rectangle in (b)).

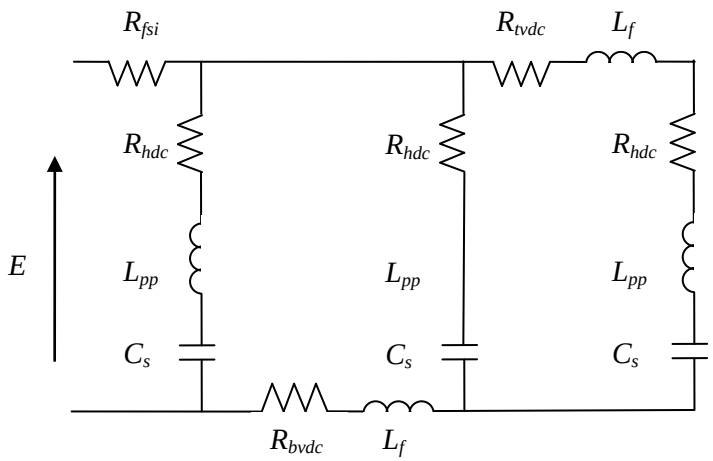

R_{fsi}: Free space impedance

R_{hdc}: Horizontal dc resistance

R_{tvdc}: Top vertical DC resistance

R_{bvdc}: Bottom vertical DC resistance

L_f: Maximum fringing inductance due to vertical side

L_{pp}: Parallel plate inductance

C_s: Series capacitance

Figure 3. Electrical circuit equivalent of the paired *S*

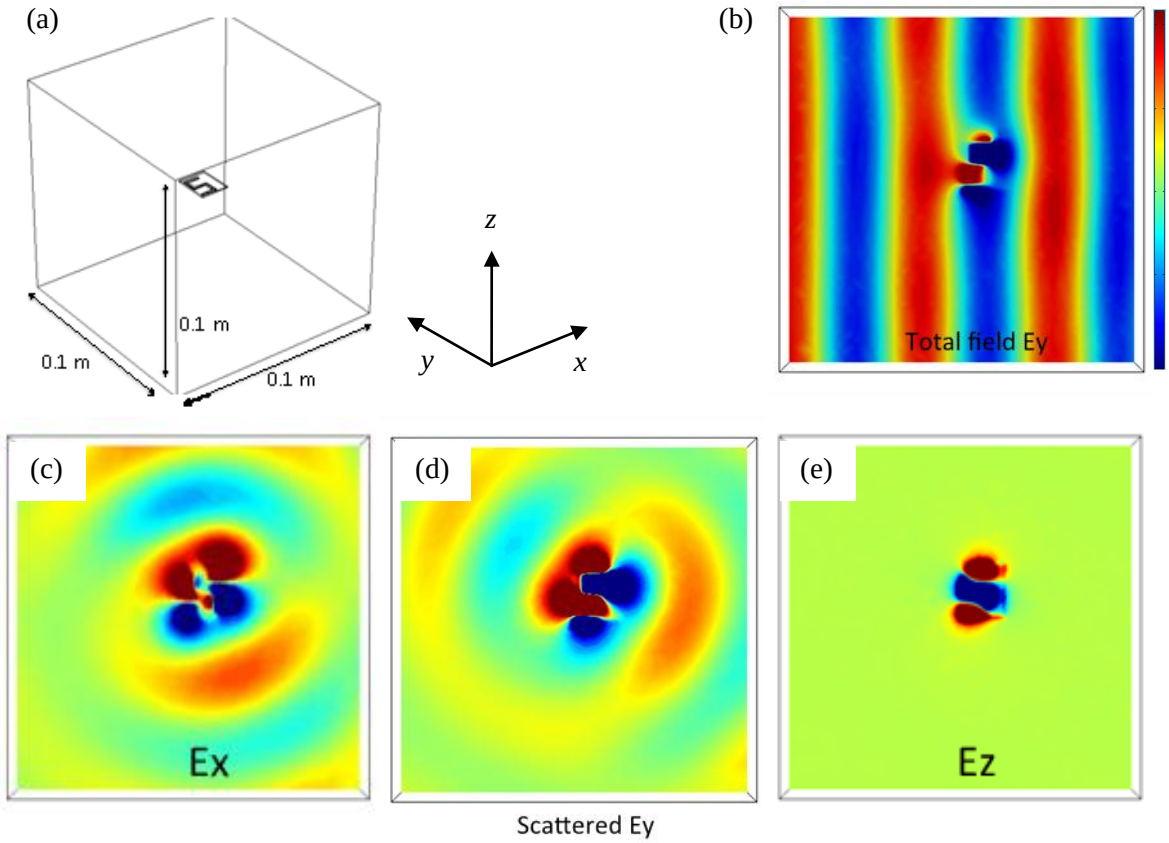

Figure 4. (a) Simulation domain (air) and the single isolated meta-atom for our study in 3D; (b) the total field (a combination of the incident field and the scattered field) of E_y assuming a plane wave is incident from the right; (c)~(e) Complex scattered field patterns of E_x, E_y, and E_z, respectively. The operating frequency in this example is at 7.83 GHz where a negative index is expected. The field distributions are displayed with the common amplitude scale indicated.

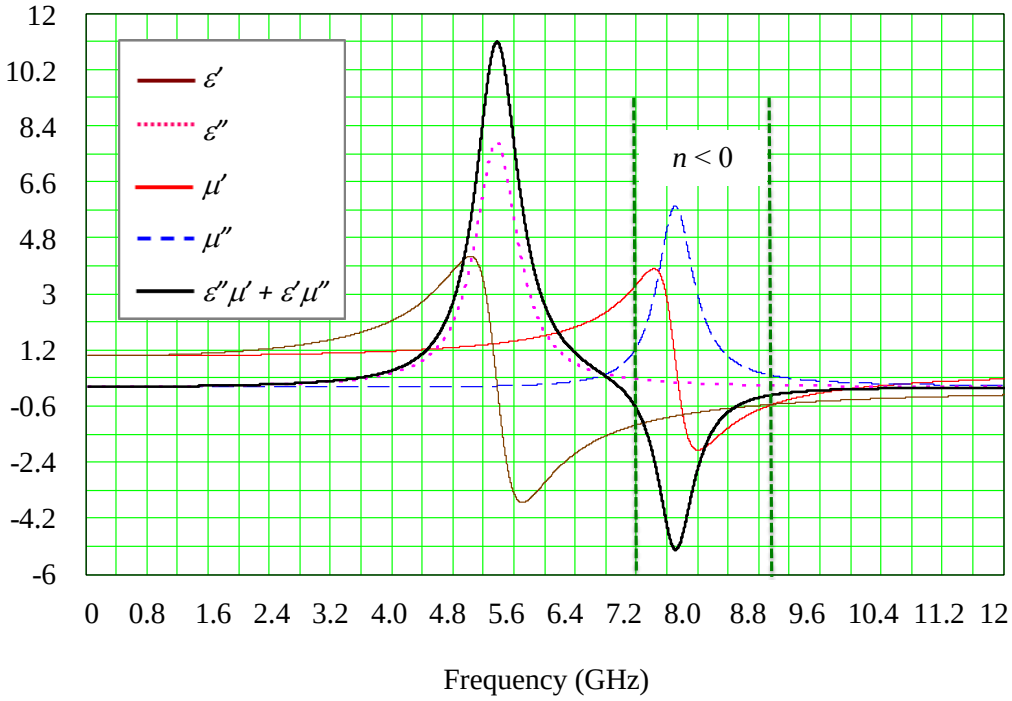

Figure 5. Estimate of real and imaginary parts of ε and μ for a single *S* meta-atom; the black curve indicates the spectral range for which a backward wave would be expected wherever it is less than zero.

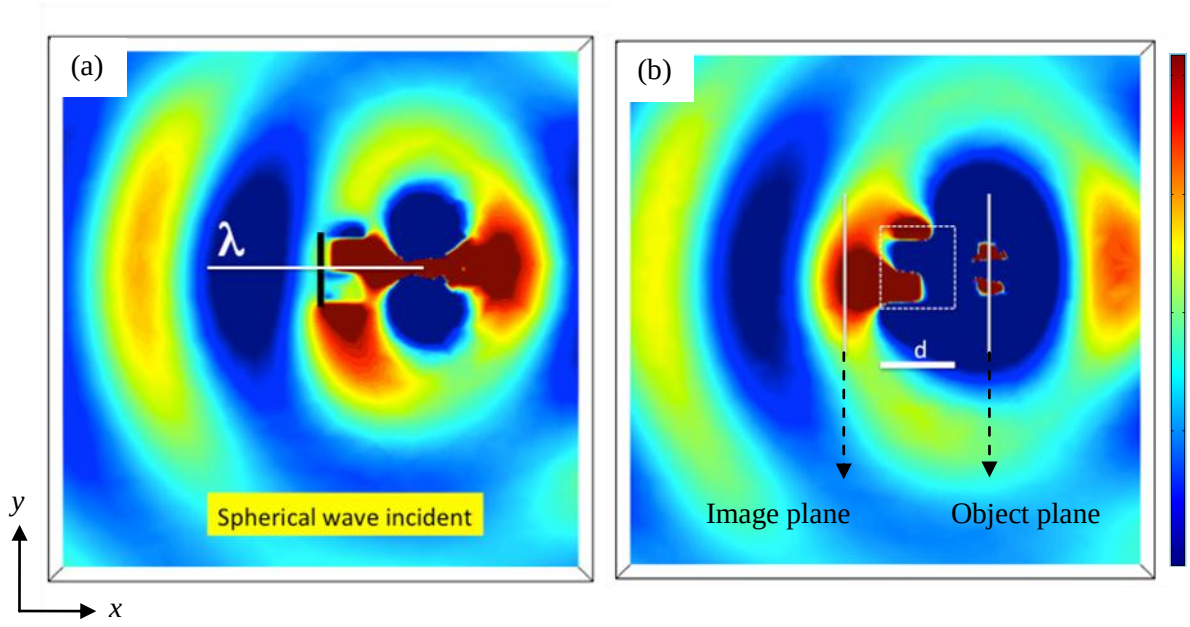

Figure 6. Scattered field patterns from a sub-wavelength *S* meta-atom with spherical wave incident from the right of the meta-atom; (a) The height of the meta-atom and the length of the wavelength are indicated by the black line and the white line respectively; (b) a low pass filtered image (on the left of the meta-atom) is displayed. The field distributions are displayed with the common amplitude scale indicated.

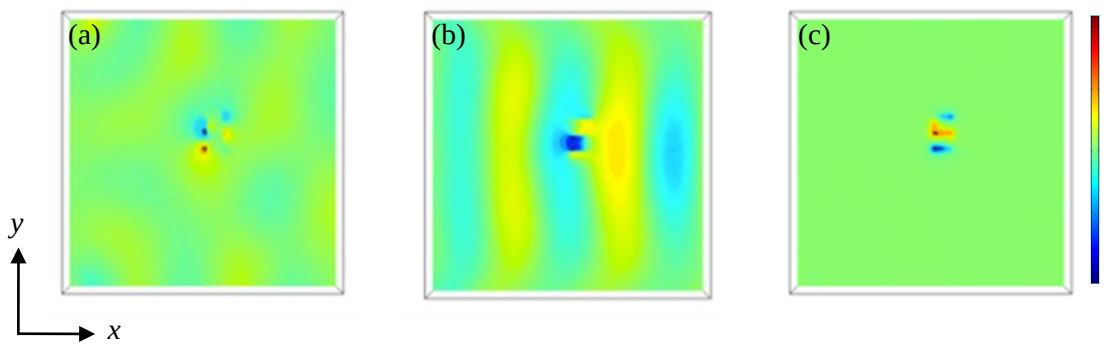

Figure 7. Scattered field patterns generated by the S meta-atom when stimulated by an evanescent wave on the left at the same frequency as used in figure 6. (a), (b), (c) display E_x, E_y, E_z, respectively. We see the creation of a propagating wave in E_y, whose spatial properties are the same for all of the $k_x > k_0$ values used. In this example, $k_x = 5k_0$. This suggests that at least for a single meta-atom there is no obvious preservation of the high spatial frequency information associated with those evanescent waves. The field distributions are displayed with the common relative amplitude scale indicated.

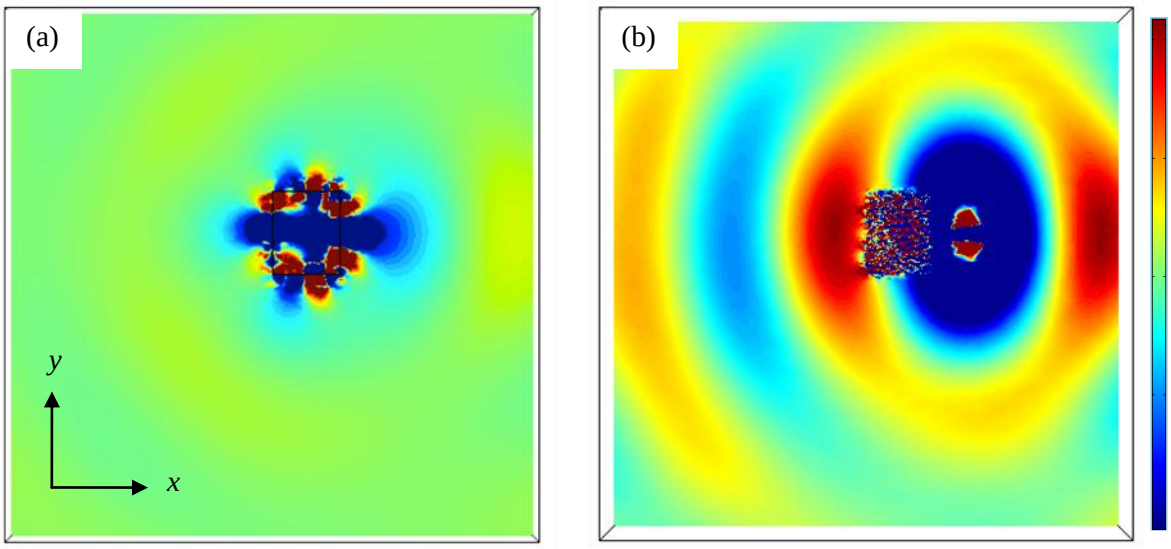

Figure 8. Images of a point source (on right of slab) using a n = -1 slab having the same dimensions as the substrate for our meta-atom; (a) cross-section at the middle of the slab (z=0); (b) cross-section at the top surface of the slab (z = 0.25 mm). There is evidence of higher spatial frequencies from the point source being transferred via surface waves to the image domain, which appears poorly resolved. This is less a limitation of the physical dimensions of the meta-atom but more a consequence of the first Born approximation. The total field is the scattered field from the slab plus the much stronger propagating dipole field from the object. The field distributions are displayed with the relative amplitude scale indicated.

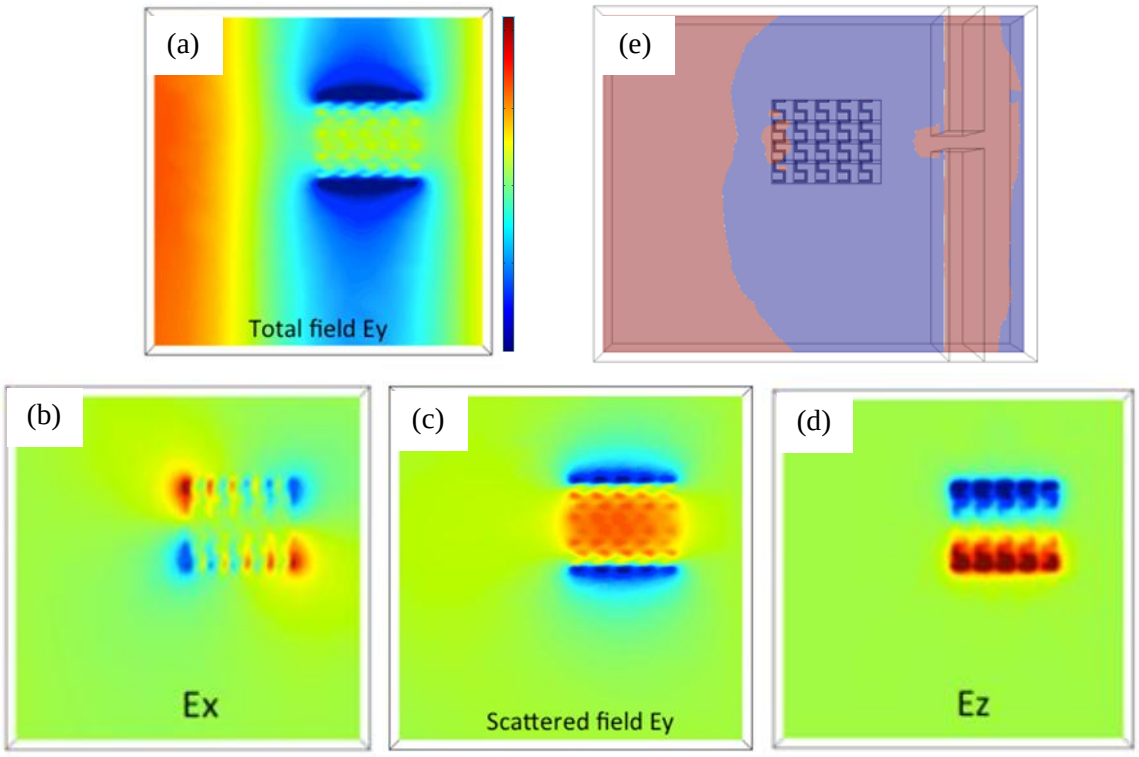

Figure 9. (a) The total field E_y from an array of 4 by 5 meta-atoms; (b)~(d) the scattered fields from the same meta-atom array. There is almost complete cancellation of the incident field by the resonantly enhanced scattered field over the surface of the 4 by 5 array; (e) an apparent image of the field from a slit following severe thresholding, but this apparent focusing of the field inside the array 3D is not due to a negative index since no backward wave is observed. The field distributions in (a) through (d) are displayed with the common scale indicated.